Materials Science Forum Vols. 558-559 (2007) pp. 641-647
online at http://www.scientific.net

Orientation Distribution of Σ3 Grain Boundary Planes in Ni Before and After Grain Boundary Engineering

H.M. Miller[1], C.-S. Kim[1], J. Gruber[1], V. Randle[2], and G.S. Rohrer[1]

[1]Department of Materials Science & Engineering, Carnegie Mellon University, Pittsburgh, PA 15213, U. S. A.
[2]Materials Research Centre, School of Engineering, University of Wales Swansea, Swansea SA2 8PP, UK.

Keywords: Grain Boundary Engineering, Grain Boundary Character Distribution, Grain Boundary Planes, Orientation Imaging Microscopy, Twins.

Abstract. The distribution of grain boundary plane orientations in polycrystalline Ni has been measured before and after grain boundary engineering. The grain boundary engineered microstructure has a relatively higher concentration of Σ3 grain boundaries and, when compared to the initial structure, more of these boundaries have orientations that are inclined by more than 10° from the (111) orientation of the ideal coherent twin. Although the conventionally measured grain size is not affected by the grain boundary engineering process, the average size of the regions containing only $\Sigma 3^n$ grain boundaries increases by nearly a factor of two. The observations indicate that the increase in the relative population of Σ3 grain boundaries results both from the preferential elimination of random grain boundaries and the generation of new Σ3 grain boundaries which do not have (111) grain boundary plane orientations.

Introduction

Iterative thermomechanical processing is a well known method of manipulating the grain boundary character distribution (GBCD) of face centered cubic metals and alloys. When the repeated cycles consist of relatively small levels of deformation and relatively low temperature annealing, the relative areas of grain boundaries with a 60° misorientation around the [111] axis (referred to here as Σ3 grain boundaries, according to the coincident site lattice notation) increase while maintaining an approximately constant grain size and a random texture. When this processing improves the bulk properties of the material, it is referred to as 'grain boundary engineering' (GBE) [1]. For example, GBE has been used to produce Ni alloys with reduced rates of intergranular stress corrosion cracking [2].

Improvements in properties have been associated with increases in the populations of grain boundaries with the Σ3 and $\Sigma 3^n$ (where n is 2 or 3) misorientations and, therefore, the evolution of the misorientation distribution as a function of processing has been well characterized [3]. However, the orientations of the Σ3 boundaries introduced by GBE have not been extensively studied. A recent investigation of grain boundary engineered brass indicated that the new Σ3 boundaries are mostly coherent twins, where a coherent twin is defined as a pure twist type Σ3 interface comprised to two parallel (111) planes on either side of the grain boundary [4]. In this paper, we will use the term *incoherent* Σ3 to indicate any Σ3 grain boundary whose plane is inclined by more than 10° from the ideal coherent twin orientation. The purpose of this paper is to determine the characteristics (crystallographic orientation) of the Σ3 grain boundaries introduced by the grain boundary engineering process in Ni, and how they affect the structure of the grain boundary network. The results indicate that while the misorientation distributions created by grain boundary engineering are similar in brass and Ni, the orientations of the grain boundary planes, and their effect on the structure of the polycrystalline network are very different.

Experimental

The polycrystalline Ni used in this study was obtained from Integran Technologies, Inc. The samples were provided in a reference state (before GBE) and in a final state following the GBE process. The two samples will be referred to as reference and GBE, respectively. The samples were prepared by first grinding the surface with SiC and diamond abrasives, then polishing using a vibratory chemomechanical process with a 0.05 μm SiO_2 slurry, and finally electropolishing in a chilled 9:1 methanol:perchloric acid solution.

Crystal orientation maps on planar sections were obtained using an electron backscatter diffraction (EBSD) mapping system integrated with a scanning electron microscope. Orientation maps were recorded at a 60° tilt with a 20 kV beam. The step sizes for the orientation mapping were between 2 μm and 4 μm, and were recorded over individual areas of 1 to 4 mm^2. In total, 64.0 mm^2 of the reference sample were mapped (an area containing approximately 20,000 grains) and 67.3 mm^2 of the GBE sample were mapped (an area containing approximately 25,000 grains). The orientation data were then processed to remove spurious observations using a 'grain dilation clean-up' in the OIM software. A single orientation was then assigned to each grain by averaging all of the orientations belonging to a single grain. The OIM analysis software was then used to extract 86,335 boundary line traces from the reference sample and 115,231 traces from the GBE sample. The trace data are summarized in Table 1. The grain boundary plane distribution was determined from these traces using a procedure described previously [5,6].

Table 1. Numbers and lengths of grain boundaries in reference and GBE Ni

		N %	L, μm	L, %	<L>, μm	L/A, μm^{-1}
reference	total	100	21.7×10^5	100	25.2	3.40×10^{-2}
	random	73	12.5×10^5	58	20.0	1.95×10^{-2}
	Σ3	27	9.23×10^5	42	38.9	1.44×10^{-2}
	coherent Σ3	15	6.18×10^5	28	48.3	0.97×10^{-2}
	incoherent Σ3	12	3.04×10^5	14	27.8	0.47×10^{-2}
GBE	total	100	23.8×10^5	100	20.6	3.53×10^{-2}
	random	47	8.79×10^5	37	16.3	1.31×10^{-2}
	Σ3	53	15.0×10^5	63	24.5	2.22×10^{-2}
	coherent Σ3	20	8.20×10^5	34	35.0	1.21×10^{-2}
	incoherent Σ3	33	6.77×10^5	28	18.0	1.01×10^{-2}

N = Number, L = Length, A = Area

Results

The grain boundary segments in each sample are classified in the following way. If the misorientation is within Brandon's criterion (8.7 °) of the ideal Σ3 misorientation, and the surface trace of the boundary is within 10° of orientation of the coherent twin, it is classified as a coherent twin. The tolerance of 10° was selected because this is commensurate with the resolution with which the five parameter grain boundary distribution data is discretized. If the misorientation is within Brandon's criterion of the ideal Σ3 misorientation, but the surface trace of the boundary is more than 10° from the orientation of the coherent twin, then it is classified as an incoherent Σ3. It should be noted that some of the incoherent Σ3s have traces that are coincidentally within the 10° tolerance and will be incorrectly classified as coherent. This leads to a small overestimation of the coherent twin population and an underestimation of the incoherent Σ3 population. Recognizing the small error, we will henceforth consider all those boundaries with traces less than 10° from the ideal trace to be coherent twins. If the boundary does not meet the Brandon criterion, it is considered a random boundary. We recognize that some of the boundaries that are placed in the random category could also be classified according to their special characteristics (for example, the Σ9 and Σ27 grain boundaries), but for the purposes of this paper we differentiate only the Σ3 boundaries.

The grain boundary populations based on this classification scheme are shown in Table 1. One thing that is clear from these data is that the GBE process increases the fraction of incoherent twins more than the fraction of coherent twins.

The data in Fig. 1 illustrate how the orientations of the Σ3 grain boundaries are distributed. In each case, the orientation of the observed grain boundary trace was compared to the orientation of a trace that would be expected if the boundary were an ideal coherent twin. Those boundaries with small deviation angles (less than 10°) are likely to be coherent and those with large angles are definitely incoherent. The data show that the fractional population of Σ3 grain boundaries increases by roughly the same amount at all deviation angles. As a result, the number and length fractions of incoherent Σ3s increases more than coherent twins. Note that the number fraction increase of Σ3 grain boundaries is larger than the length fraction increase because, as shown in Table 1, the Σ3 grain boundaries resulting from the GBE process have, on average, less area than the pre-existing Σ3 grain boundaries.

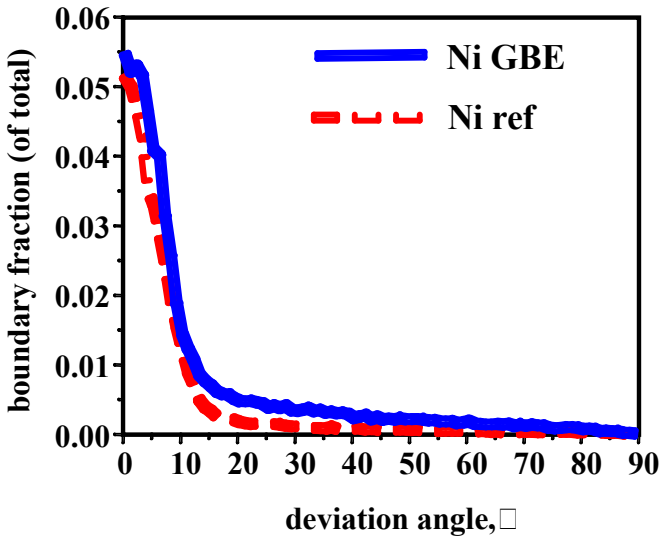

Figure 1. The fraction of Σ3 grain boundaries as a function of the angle (°) between the measured grain boundary trace and the trace expected for an ideal coherent twin. The dashed line is for the reference sample and the solid line is for the GBE sample.

The distribution of grain boundary plane orientations for Σ3 grain boundaries is strongly peaked at the orientation of the coherent twin, (111). Grain boundary planes with that orientation occur with a population of approximately 1000 times random, and because of this strong peak, it is difficult to visualize any of the features of the distribution of incoherent boundaries. For this reason, the distribution of grain boundary planes in Fig. 2 is plotted with the coherent twins excluded. Because of the exclusion of the coherent twins, the distribution appears as a crater, with a minimum at the (111) position and an annular maximum 10° away that reaches more than 200 times random. Note that the values of the distribution at the (111) position are exactly zero, even though the contouring program used to plot Fig. 2 does not accurately represent this singularity. The distributions for the reference and GBE materials are similar, except for the fact that in the GBE sample, the distributions extend further away from the ideal (111) position. Along the $[\bar{1}10]$ zone, indicated by the white line, the grain boundary plane population is greater than or equal to 30 MRD at all orientations. A more detailed comparison of the populations of the reference and GBE samples along the $[\bar{1}10]$ zone is illustrated in Fig. 3. Although the population of incoherent Σ3 grain boundaries in the reference sample approaches 1 MRD at some orientations, a relatively high population is maintained for all orientations in the $[\bar{1}10]$ zone of the GBE sample.

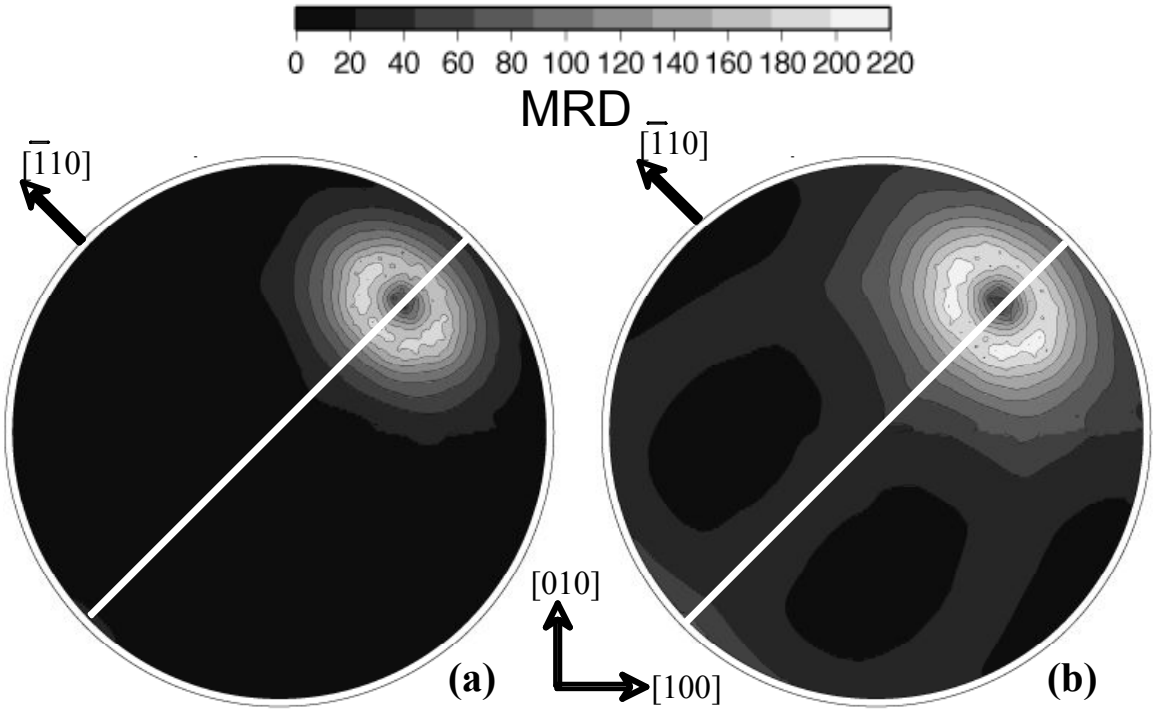

Figure 2. The distribution of grain boundary planes for the Σ3 misorientation (60° rotation about [111]), after the subtraction of coherent twins, in the (a) reference and (b) grain boundary engineered sample. In both diagrams, there are 10 contours with a spacing of 22 MRD. The white line shows the position of the [$\bar{1}$ 10] zone.

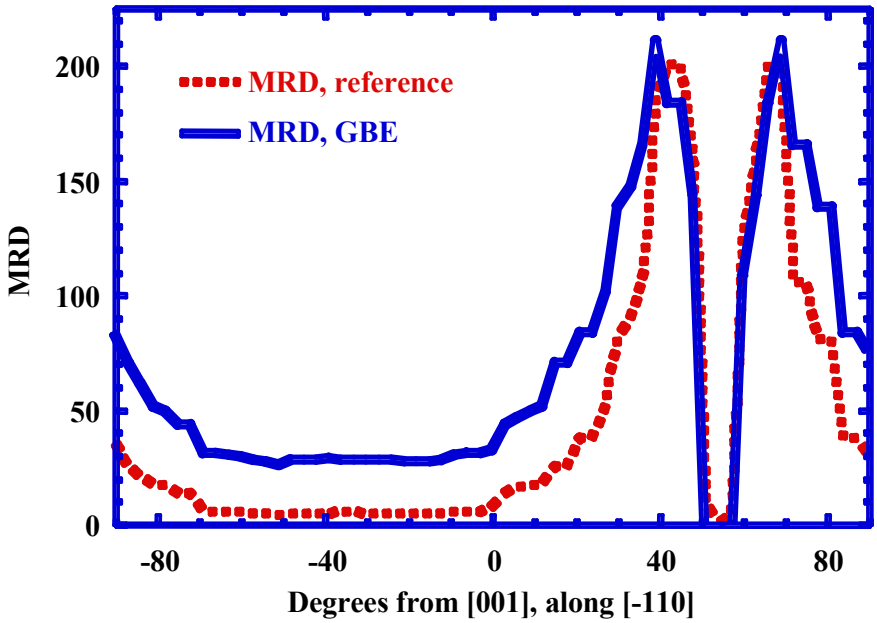

Figure 3. The population of Σ3 grain boundaries along the [$\bar{1}$ 10] zone. The dashed line is the reference sample and the solid line is the GBE sample. The coherent twins have been removed, and this accounts for the minimum at 57 ± 10°.

The microstructures of the reference and GBE samples show distinct differences (see Fig. 4). When the conventional grain sizes of the reference (Fig. 4a) and GBE (Fig. 4c) sample are determined, both are 40 μm. The identical grain sizes are consistent with the measurements of the grain boundary length per area for the two samples (see Table 1), which are also nearly the same. These observations are consistent with reports that the grain size is not altered by the grain

boundary engineering process. If coherent twins are excluded from the analysis, the average grain sizes are 49 μm and 51 μm, which are again comparable. However, if all Σ3 grain boundaries are excluded, the grain sizes are 56 μm and 104 μm. This is a measure of the size of domains within which all of the material is related by the Σ3 misorientation. To show this graphically, we can compare the microstructures with all grain boundaries (Fig. 4a and Fig. 4c) to the same areas when the $\Sigma 3^n$ grain boundaries are eliminated (Σ9 and Σ27 boundaries must be formed when two Σ3s intersect, so these grain boundaries frequently connect the Σ3 boundaries within a twin related domain). It is clear that the regions of material containing only $\Sigma 3^n$ grain boundaries are much larger in Fig. 4d. The boundary maps in Fig. 4b and 4d are consistent with the observation that the length of random boundaries per unit area decreases significantly as a result of grain boundary engineering (see Table 1).

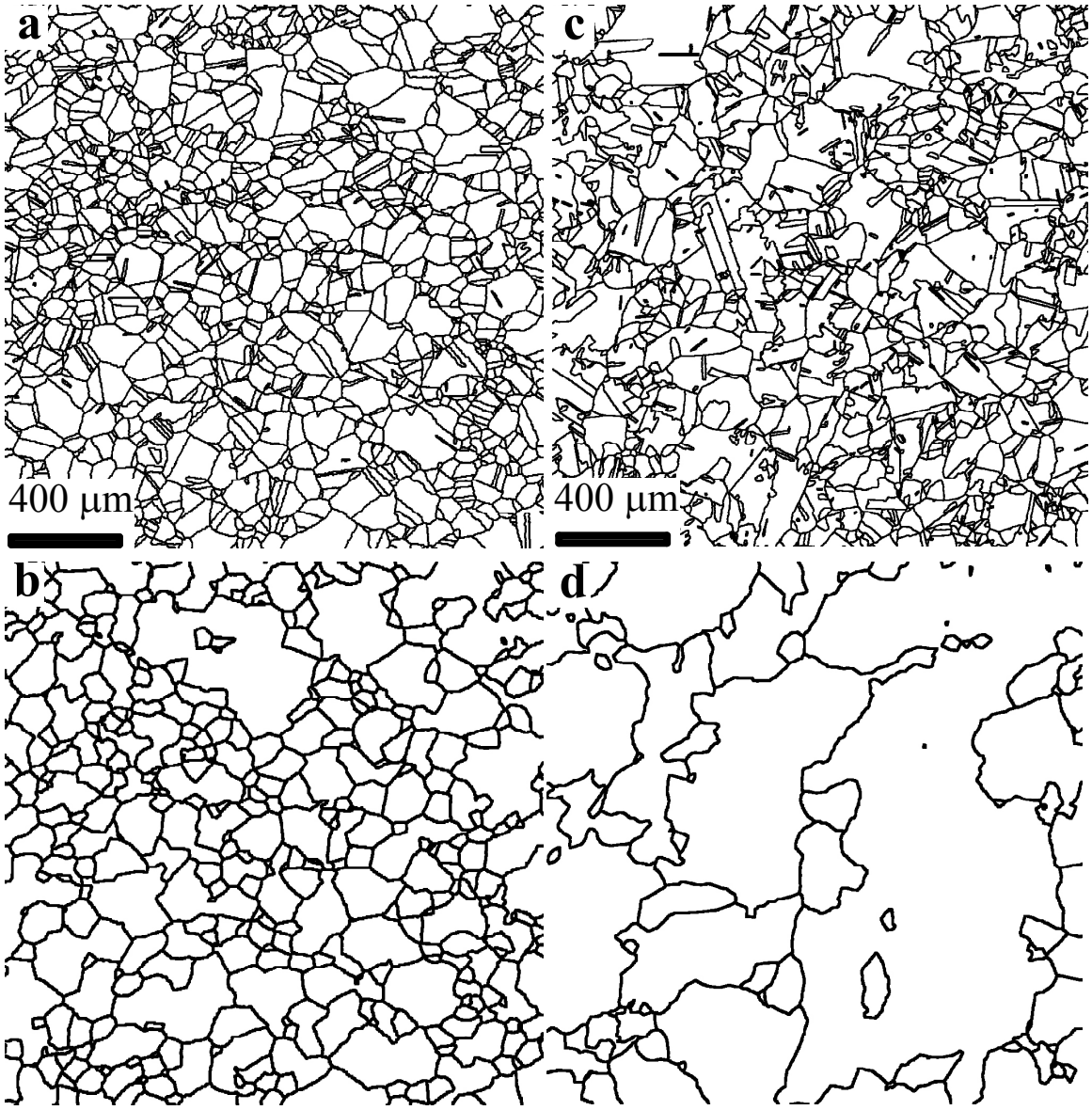

Figure 4. Grain boundary traces in 2000 μm x 2000 μm areas of the reference sample (a & b) and the GBE sample (c & d). (a) All grain boundaries in the reference sample are denoted as black lines. (b) All grain boundaries in the reference sample that are not classified as $\Sigma 3^n$. (c) All grain boundaries in the GBE sample. (d) All grain boundaries in the GBE sample that are not classified as $\Sigma 3^n$.

Discussion

During normal grain growth, grain boundary surface area is continuously eliminated to lower the total interfacial area and its associated energy. The microstructural changes that occur during grain boundary engineering are quite different in that the motion of boundaries during the brief, low temperature anneals is limited in range and occurs mainly to relieve stored strain energy. However, in analogy to normal grain growth, the total interfacial energy is decreased by replacing relatively higher energy random grain boundaries with relatively lower energy Σ3 boundaries. This is illustrated most clearly by the measurements of grain boundary length per unit area (Table 1) which show that although the total is roughly constant, the Σ3 length per area increases by 0.78 μm^{-1} and the random length per area decreases by 0.64 μm^{-1}. This results in the growth of the twin related domains, as shown in Fig. 4c and 4d.

It is important to remember that because the changes in the grain boundary character distribution are frequently reported as fractional quantities, there are two ways of increasing the relative populations of Σ3 grain boundaries. One is to create more of these boundaries. The second is to decrease the concentrations of the other, random boundaries, while simply maintaining roughly the same number of Σ3 boundaries. As a highly simplified example, consider a microstructure with 100 boundaries, 25 of which are Σ3 and 75 of which are not. If two thirds of the non- Σ3 boundaries are eliminated, then the concentration of Σ3 grain boundaries increases from 25% to 50% without producing any new Σ3s. By considering the grain boundary area per length, as above, it appears that both of these mechanisms are important for the formation of the microstructure in GBE Ni. For example, the comparison of Fig. 4c and 4d clearly shows that the elimination of non-$\Sigma 3^n$ grain boundaries is occurring. This is consistent with an observed decrease in the length of non-$\Sigma 3^n$ grain boundary trace per unit area. At the same time, additional incoherent Σ3 boundaries are created, as illustrated in Figs. 1-3. In other words, while the grain boundary engineering process does create additional Σ3 boundaries, it is also effective in reducing the numbers of non- $\Sigma 3^n$ boundaries.

This elimination of the random boundaries means that more Σ3s intersect, and this necessarily generates Σ9 and Σ27 boundaries [7,8]. Because these $\Sigma 3^n$ boundaries must create a network, it is not always possible for the Σ3 boundaries to lie on their ideal plane. The constraints imposed by the orientations of pre-existing twins and the need for interfacial equilibrium at the triple junction forces some of these boundaries to adopt non-ideal grain boundary planes. The high population of incoherent Σ3s that fall on the $[\bar{1}10]$ zone (and equivalent zone axes perpendicular to the [111] direction) is likely to be related to topological constraints for the following reason. The Σ3, Σ9, and Σ27a boundaries all have common [110] axes. Our studies of the grain boundary plane distribution of these boundary types (not presented here) shows that as was the case for brass [4], most of these grain boundaries can be classified as pure [110] tilt boundaries. An analysis of the triple junction types shows that 40 % are made up of these three boundaries types and if two of them are tilt boundaries, then the common [110] axis constrains the third boundary plane to be in the [110] zone.

Previous work has shown that there is an inverse correlation between grain boundary energy and grain boundary areas and populations [9-11]. It has also been established that the energies of Σ3 grain boundaries increase significantly for rotations away from the ideal twin configuration [12-13]. Therefore, the observations that incoherent Σ3s have lower average areas and a smaller length per unit area than the coherent twins (see Table 1) are consistent with the inverse correlation between grain boundary energy and area.

Finally, it should be recognized that the observations in Ni are very different from previous observations in brass [4]. In the case of brass, nearly all of the new Σ3 boundaries were coherent twins that spanned distinct grains without interruption. This is the opposite of what is observed here, where collections of interconnected $\Sigma 3^n$ boundaries form networks within twin related domains. There are several factors that are likely to be responsible for the differences between Ni

and brass. First, brass has a lower stacking fault energy than Ni, so annealing twin formation is more likely [14]. Second, the formation of annealing twins can be temperature dependent, so differences in the annealing conditions could also be responsible for different concentrations of annealing twins [15].

Conclusion

Grain boundary engineered Ni has a relatively higher concentration of Σ3 grain boundaries and, when compared to the initial structure, more of these boundaries have orientations that are inclined by more than 10° from the {111} orientation of the ideal coherent twin. The grain boundary engineering process also increases the average size of the regions containing only $\Sigma 3^n$ grain boundaries by nearly a factor of two. The observations indicate that the increase in the relative population of Σ3 grain boundaries results both from the preferential elimination of random grain boundaries and the generation of new, incoherent Σ3 grain boundaries.

Acknowledgements

The work at Carnegie Mellon University was supported primarily by the MRSEC program of the National Science Foundation under Award Number DMR-0520425. The work at Swansea was partially supported by the Engineering and Physical Sciences Research Council.

References

[1] Viewpoint set no. 40, Grain boundary engineering, Edited by M. Kumar and C.A. Schuh, Scripta Mater. 54 (2006), p. 961.
[2] P. Lin, G. Palumbo, U. Erb, K.T. Aust: Scripta Metall. et Mater. Vol. 33 (1995), p. 1387.
[3] V. Randle: Acta Mater. Vol. 52 (2004), p. 4067.
[4] G.S. Rohrer, V. Randle, C.-S. Kim, Y. Hu: Acta Mater. Vol. 54 (2006) p. 4389.
[5] D.M. Saylor, B.S. El-Dasher, B.L. Adams, G.S. Rohrer: Metall. and Mater. Trans., Vol. 35A (2004) p. 1981.
[6] G.S. Rohrer, D.M. Saylor, B.S. El-Dasher, B.L. Adams, A.D. Rollett, P. Wynblatt: Z. Metall., Vol. 95 (2004) p. 197.
[7] K. Miyazawa, Y. Iwasaki, K. Ito, Y. Ishida: Acta Cryst. Vol. A52 (1996) p. 787.
[8] L.C. Lim, R. Raj: Acta Metall. Vol. 32 (1984) p. 1177.
[9] D.M. Saylor, A. Morawiec, G.S. Rohrer, Acta Mater.: Vol. 51 (2003) p. 3675.
[10] D.M. Saylor, B.S. El-Dasher, T. Sano, G.S. Rohrer: J. Amer. Ceram. Soc., Vol. 87 (2004) p. 670.
[11] D.M. Saylor, B.S. El Dasher, A.D. Rollett, G.S. Rohrer: Acta Mater: Vol. 52 (2004) p. 3649.
[12] R. Schmelzle, T. Muschik, W. Gust, B. Predel: Scripta Metall et Mater Vol. 25 (1991) p. 1981.
[13] U. Wolf, F. Ernst T. Muschik, M.W. Finnis, H.F. Fischmeister: Phil Mag A Vol. 66 (1992) p. 991.
[14] J.W. Christian, P.R. Swann, in: *Alloying behavior and effects in concentrated solid solutions.* New York (NY): Gordon & Breach Sci. Pub.; 1965. p.105
[15] H. Gleiter: Acta Metall Vol. 17 (1969) p. 1421.